

# Microemulsion Templating of Siliceous Mesostructured Cellular Foams with Well-Defined Ultralarge Mesopores

Patrick Schmidt-Winkel,<sup>†,‡</sup> Wayne W. Lukens, Jr.,<sup>†,‡</sup> Peidong Yang,<sup>†</sup>  
David I. Margolese,<sup>†</sup> John S. Lettow,<sup>§</sup> Jackie Y. Ying,<sup>\*,§</sup> and Galen D. Stucky<sup>\*,†,‡</sup>

Department of Chemistry and Materials Research Laboratory, University of California, Santa Barbara, California 93106, and Department of Chemical Engineering, Massachusetts Institute of Technology, Cambridge, Massachusetts 02139

Received July 8, 1999. Revised Manuscript Received November 3, 1999

Siliceous mesostructured cellular foams (MCFs) with well-defined ultralarge mesopores and hydrothermally robust frameworks are described. The MCFs are templated by oil-in-water microemulsions and are characterized by small-angle X-ray scattering, nitrogen sorption, transmission electron microscopy, scanning electron microscopy, thermogravimetry, and differential thermal analysis. The MCFs consist of uniform spherical cells measuring 24–42 nm in diameter, possess BET surface areas up to 1000 m<sup>2</sup>/g and porosities of 80–84%, and give, because of their pores with small size distributions, higher-order scattering peaks even in the absence of long-range order. Windows with diameters of 9–22 nm and narrow size distribution interconnect the cells. The pore size can be controlled by adjusting the amount of the organic swelling agent that is added and by varying the aging temperature. Adding ammonium fluoride selectively enlarges the windows by 50–80%. In addition, the windows can be enlarged by postsynthesis treatment in hot water. The MCF materials resemble aerogels, but offer the benefits of a facilitated synthesis in combination with well-defined pore and wall structure, thick walls, and high hydrothermal stability. The open system of large pores give MCFs unique advantages as catalyst supports and separation media for processes involving large molecules, and the high porosities make them of interest for electrical and thermal insulation applications.

## Introduction

Molecular sieves with uniform and well-defined pores are promising materials for a variety of applications in catalysis, separations, etc.<sup>1</sup> Mesoporous materials with well-defined pore sizes of 2–50 nm can be prepared utilizing the self-aggregation properties of various surfactants.<sup>2</sup> Amphiphilic block copolymers have turned out to be valuable supramolecular templates for creating mesostructured materials possessing long-range order.<sup>3</sup> Aside from employing different types of surfactants,<sup>2</sup> the pore sizes of mesoporous materials have been controlled

by changing the hydrophobic volumes of the templates, which may be achieved by changing the reaction temperature or by adding organic cosolvents as swelling agents.<sup>3c,d,4</sup> More recently developed strategies for obtaining well-defined macroporous and large-pore mesoporous materials use colloidal templating methods, in which either emulsions<sup>5a,b</sup> or polymer latex spheres<sup>6a–e,g</sup> are utilized as templates. However, mesoporous materials with well-defined ultralarge pores (30–50 nm) have been difficult to obtain by existing synthetic methods.<sup>3f,6c</sup>

\* To whom correspondence should be addressed. G.D.S.: phone, (805) 893-4872; fax, (805) 893-4120; e-mail, stucky@chem.ucsb.edu. J.Y.Y.: phone, (617) 253-2899; fax, (617) 258-5766; e-mail, jyying@mit.edu.

<sup>†</sup> Department of Chemistry, University of California.

<sup>‡</sup> Materials Research Laboratory, University of California.

<sup>§</sup> Massachusetts Institute of Technology.

(1) (a) Perry, R. H.; Green, D. In *Perry's Chemical Engineers' Handbook*; Perry, R. H., Green, D., Eds.; McGraw-Hill: New York, 1984. (b) Hearn, M. T. W. *HPLC of Proteins, Peptides and Polynucleotides*; VCH: New York, 1991. (c) Davis, M. E. *Chem. Ind.* **1992**, 4, 137. (d) Blasco, T.; Corma, A.; Navarro, M. T.; Pérez Pariente, J. *J. Catal.* **1995**, 156, 65. (e) Gontier, S.; Tuel, E. *Zeolites* **1995**, 15, 601. (f) Maschmeyer, T.; Rey, F.; Sankar, G.; Thomas, J. M. *Nature* **1995**, 378, 159. (g) Zhang, W.; Wang, J.; Tanev, P. T.; Pinnavaia, T. J. *Chem. Commun.* **1996**, 979. (h) Walker, J. V.; Morey, M.; Carlsson, H.; Davidson, A.; Stucky, G. D.; Butler, A. J. *Am. Chem. Soc.* **1997**, 119, 6921. (i) Feng, X.; Fryxell, G. E.; Wang, L.-Q.; Kim, A. J.; Liu, J.; Kemner, K. M. *Science* **1997**, 276, 923. (j) Mercier, L.; Pinnavaia, T. J. *Adv. Mater.* **1997**, 9, 500.

(2) For recent reviews, see: (a) Ying, J. Y.; Mehnert, C. P.; Wong, M. S. *Angew. Chem., Int. Ed.* **1999**, 38, 56. (b) Ciesla, U.; Schüth, F. *Microporous Mesoporous Mater.* **1999**, 27, 131.

(3) (a) Bagshaw, S. A.; Prouzet, E.; Pinnavaia, T. J. *Science* **1995**, 269, 1242. (b) Templin, M.; Franck, A.; Du Chesne, A.; Leist, H.; Zhang, Y.; Ulrich, R.; Schädler, V.; Wiesner, U. *Science* **1997**, 278, 1795. (c) Zhao, D.; Feng, J.; Huo, Q.; Melosh, N.; Fredrickson, G. H.; Chmelka, B. F.; Stucky, G. D. *Science* **1998**, 279, 548. (d) Zhao, D.; Huo, Q.; Feng, J.; Chmelka, B. F.; Stucky, G. D. *J. Am. Chem. Soc.* **1998**, 120, 6024. (e) Göltner, C. G.; Henke, S.; Weissenberger, M. C.; Antonietti, M. *Angew. Chem., Int. Ed.* **1998**, 37, 613. (f) Krämer, E.; Förster, S.; Göltner, C.; Antonietti, M. *Langmuir* **1998**, 14, 2027. (g) Göltner, C. G.; Berton, B.; Krämer, E.; Antonietti, M. *Chem. Commun.* **1998**, 2287. (h) Zhao, D.; Yang, P.; Melosh, N.; Feng, J.; Chmelka, B. F.; Stucky, G. D. *Adv. Mater.* **1998**, 10, 1380. (i) Yang, P.; Zhao, D.; Chmelka, B. F.; Stucky, G. D. *Chem. Mater.* **1998**, 10, 2033. (j) Yang, P.; Zhao, D.; Margolese, D. I.; Chmelka, B. F.; Stucky, G. D. *Nature* **1998**, 396, 152. (k) Ulrich, R.; Du Chesne, A.; Templin, M.; Wiesner, U. *Adv. Mater.* **1999**, 11, 141. (l) Schmidt-Winkel, P.; Yang, P.; Margolese, D. I.; Chmelka, B. F.; Stucky, G. D. *Adv. Mater.* **1999**, 11, 303. (m) Zhao, D.; Yang, P.; Chmelka, B. F.; Stucky, G. D. *Chem. Mater.* **1999**, 11, 1174. (n) Lu, Y.; Fan, H.; Stump, A.; Ward, T. L.; Rieker, T.; Brinker, C. J. *Nature* **1999**, 398, 223.

(4) (a) Beck, J. S.; Vartuli, J. C.; Roth, W. J.; Leonowicz, M. E.; Kresge, C. T.; Schmitt, K. D.; Chu, C. T. W.; Olson, D. H.; Sheppard, E. W.; McCullen, S. B.; Higgins, J. B.; Schlenker, J. L. *J. Am. Chem. Soc.* **1992**, 114, 10834. (b) Huo, Q.; Leon, R.; Petroff, P. M.; Stucky, G. D. *Science* **1995**, 268, 1324. (c) Prouzet, E.; Pinnavaia, T. J. *Angew. Chem., Int. Ed.* **1997**, 36, 516.

Inspired by our earlier work on the use of surfactant-stabilized emulsions to template mesoporous spherical shells<sup>15</sup> and hard spheres<sup>16</sup> and by the more recent colloidal templating of well-defined, porous materials,<sup>5a,b,6</sup> we have recently developed microemulsions as colloidal templates for porous solids.<sup>7,8</sup> This new templating route has enabled the facile and efficient preparation of mesostructured cellular foam (MCF) materials.<sup>7</sup> The MCFs represent a new class of aerogel-like, three-dimensional, continuous, ultralarge-pore mesoporous materials that can be synthesized easily with well-controlled, uniformly sized and shaped pores. In this paper we present detailed studies of the MCF materials. This work is part of our ongoing research program to create patterned porous and composite structures with dimensions in the range of 10–100 nm.<sup>3c,d,h,i,l,m,6e</sup>

## Experimental Section

**Measurements.** Small-angle X-ray scattering (SAXS) experiments were performed in the transmission mode on a Scintag PADX diffractometer (Cu K $\alpha$  radiation) equipped with a Si(Li) solid-state detector cooled by a Peltier cell. The SAXS data were processed as described in the X-ray scattering section of this paper (see below). Nitrogen sorption analyses were carried out with a Micromeritics ASAP 2000 porosimeter at  $-196$  °C on samples that had been degassed at  $180$  °C under high vacuum for at least 4 h. The data were analyzed according to a modified Broekhoff–de Boer method by using Hill's approximation for the thickness of the adsorbed gas layer.<sup>9</sup> Brunauer–Emmett–Teller (BET)<sup>10</sup> surface area measurements were performed over a relative pressure range of 0.05–0.16.<sup>11</sup> Scanning electron microscopy (SEM) was carried out on a JEOL 6300-F microscope equipped with a field-emission gun operating at 3.0 kV acceleration voltage. The SEM samples were sputter-coated with a thin layer of Au/Pd. Transmission electron microscopy (TEM) of samples deposited on carbon–copper grids was performed on a JEOL 2000 microscope operating at 200 kV (LaB<sub>6</sub> filament). Simultaneous thermogravimetric and differential thermal analyses (TGA/DTA) were carried out in air on a Netzsch STA 409 thermoanalyzer with a heating rate of 5 K/min, using alumina as the reference. Solid-state <sup>29</sup>Si MAS NMR spectra were recorded on a General Electric GN-300 spectrometer with a Tecmag console operating at a <sup>29</sup>Si resonance frequency of 59.71 MHz under conditions of magic-angle spinning at room temperature and with tetramethylsilane as the reference.

**Materials.** All materials were used as received from the chemical vendors without further purification. Water used in the MCF syntheses was deionized.

**General Procedure for Microemulsion Templating of MCF Materials.** The MCFs are prepared in aqueous hydro-

chloric acid using dilute solutions of the nonionic block copolymer surfactant Pluronic P123 (poly(ethylene oxide)-*block*-poly(propylene oxide)-*block*-poly(ethylene oxide), EO<sub>20</sub>–PO<sub>70</sub>–EO<sub>20</sub>,  $M_{av} = 5800$ ) with 1,3,5-trimethylbenzene (TMB) as the organic swelling agent. To control the pore sizes in the MCFs, the TMB concentration is varied while the amount of P123 is kept constant. Thus, the amount of TMB used is expressed in terms of TMB/P123 weight ratios.<sup>7,8</sup> In a typical preparation, P123 (2.0 g, 0.4 mmol) is dissolved in 1.6 M HCl (75 mL, 120 mmol HCl) at room temperature while being stirred in a beaker covered with a watch glass. TMB (2.0 g, 17 mmol) and—if desired—NH<sub>4</sub>F<sup>31</sup> (23 mg, 0.6 mmol) are then added, and the mixture is heated to 37–40 °C. Following 0–65 min of stirring, tetraethyl orthosilicate (TEOS; 4.4 g, 21 mmol) is added. After 20 h at 37–40 °C, the milky reaction mixture is transferred to an autoclave and aged at 100 or 120 °C for 24 h under static conditions. The mixture is then allowed to cool to room temperature, and the white precipitate is isolated by filtration, dried in air for at least 2 days, and calcined at 500 °C for 8 h in air to produce the MCF materials. Typical yields are 94–100% based on Si.

## Results and Discussion

### Synthesis of Mesostructured Cellular Foams.

The MCFs are formed at a pH below the aqueous isoelectric point of silica.<sup>12</sup> In this regard, the procedure is analogous to that currently used to create porous silica structures that have two- and three-dimensional periodicities with long-range order on mesoscopic and macroscopic length scales in the form of powders, fibers, spheres, thin films, and monoliths.<sup>3b–e,h–n,13</sup> The acid-catalyzed synthesis of nonordered silica has been known to introduce a large number of residual surface hydroxy groups,<sup>14</sup> which may facilitate further functionalization of the MCFs. We have utilized oil-in-water microemulsions<sup>7,8</sup> to template the MCFs. The easily prepared microemulsion templates consist of water, Pluronic P123 (EO<sub>20</sub>–PO<sub>70</sub>–EO<sub>20</sub>), and 1,3,5-trimethylbenzene (TMB) as the organic cosolvent (oil). The nonionic block copolymer surfactant P123 forms expandable aggregates that template periodic SBA-15-type mesoporous silica in acidic media,<sup>3c,d,h,i,l,m,6e</sup> and is well suited for stabilizing oil-in-water and oil-in-formamide emulsions<sup>5</sup> and oil-in-water microemulsions.<sup>8</sup> To the oil-in-water microemulsions is added tetraethyl orthosilicate (TEOS) as the source of both silica and ethanol (which acts as a cosurfactant<sup>8</sup>). After the synthesis mixtures are kept at 37–40 °C for 1 day, followed by aging at 100 or 120 °C for 1 day, the precipitates are isolated by filtration, allowed to dry at room temperature, and then calcined to give the MCFs.

Two important aspects of the microemulsion templating route are its simplicity and efficiency. Aqueous emulsions have been used previously to control the macroscopic morphologies of mesoporous fibers,<sup>15</sup> hollow mesoporous spheres,<sup>15</sup> and discrete spherical particles

(5) (a) Imhof, A.; Pine, D. J. *Nature* **1997**, *389*, 948. (b) Imhof, A.; Pine, D. J. *Adv. Mater.* **1998**, *10*, 697. (c) Imhof, A.; Pine, D. J. *Adv. Mater.* **1999**, *11*, 311.

(6) (a) Velev, O. D.; Jede, T. A.; Lobo, R. F.; Lenhoff, A. M. *Nature* **1997**, *389*, 447. (b) Velev, O. D.; Jede, T. A.; Lobo, R. F.; Lenhoff, A. M. *Chem. Mater.* **1998**, *10*, 3597. (c) Antonietti, M.; Berton, B.; Göltner, C.; Hentze, H.-P. *Adv. Mater.* **1998**, *10*, 154. (d) Holland, B. T.; Blanford, C. F.; Stein, A. *Science* **1998**, *281*, 538. (e) Yang, P.; Deng, T.; Zhao, D.; Feng, P.; Pine, D.; Chmelka, B. F.; Whitesides, G. M.; Stucky, G. D. *Science* **1998**, *282*, 2244. (f) Davey, R. J.; Alison, H.; Cilliers, J. J.; Garside, J. *Chem. Commun.* **1998**, 2581. (g) Holland, B. T.; Blanford, C. F.; Do, T.; Stein, A. *Chem. Mater.* **1999**, *11*, 795.

(7) Schmidt-Winkel, P.; Lukens, W. W., Jr.; Zhao, D.; Yang, P.; Chmelka, B. F.; Stucky, G. D. *J. Am. Chem. Soc.* **1999**, *121*, 254.

(8) Schmidt-Winkel, P.; Glinka, C. J.; Stucky, G. D. *Langmuir*, in press.

(9) Lukens, W. W., Jr.; Schmidt-Winkel, P.; Zhao, D.; Feng, J.; Stucky, G. D. *Langmuir* **1999**, *15*, 5403.

(10) Brunauer, S.; Emmett, P.; Teller, E. *J. Am. Chem. Soc.* **1938**, *60*, 309.

(11) Gregg, S. J.; Sing, K. S. W. In *Adsorption, Surface Area and Porosity*; Academic Press: New York, 1982.

(12) Huo, Q.; Margolese, D. I.; Ciesla, U.; Feng, P.; Gier, T. E.; Sieger, P.; Leon, R.; Petroff, P. M.; Schüth, F.; Stucky, G. D. *Nature* **1994**, *368*, 317.

(13) (a) For a recent review, see: Zhao, D.; Yang, P.; Huo, Q.; Chmelka, B. F.; Stucky, G. D. *Curr. Opin. Solid State Mater. Sci.* **1998**, *3*, 111. (b) Yang, S. M.; Yang, H.; Coombs, N.; Sokolov, I.; Kresge, C. T.; Ozin, G. A. *Adv. Mater.* **1999**, *11*, 52. (c) Lin, H.-P.; Liu, S.-B.; Mou, C.-Y.; Tang, C.-Y. *Chem. Commun.* **1999**, 583. (d) Wang, L.-Z.; Shi, J.-L.; Tang, F.-Q.; Yu, J.; Ruan, M.-L.; Yan, D.-S. *J. Mater. Chem.* **1999**, *9*, 643.

(14) Brinker, C. J.; Scherer, G. W. In *Sol–Gel Science: The Physics and Chemistry of Sol–Gel Processing*; Academic Press: San Diego, 1990.

with mesoporosity;<sup>16</sup> the pores, however, are not directly affected by the emulsions. More analogous to our synthesis route is the use of nonaqueous, fractionated emulsions for the preparation of macroporous oxides and organic polymers with uniform pores.<sup>5a,b</sup> Characterization of the MCFs (see below) shows that their mesopores consist of quite uniform cells and windows. We use the microemulsions directly, without further processing such as fractionation, to template the MCFs. This indicates that the use of microemulsions, which are more thermodynamically stable than emulsions,<sup>17</sup> circumvents the need for fractionation<sup>5a,b</sup> to produce uniform pores.

Macroporous and ultralarge-pore mesoporous materials can be prepared by using polymer latex spheres<sup>6a–e,g</sup> or ionic block copolymers<sup>3f</sup> as templates. These techniques require the time-consuming and nontrivial synthesis of polymeric templates. In addition, uniform pore sizes have been achieved only for macroporous materials,<sup>6a,b,d,e,g</sup> whereas the ultralarge-pore mesoporous materials have bimodal or polydisperse pore size distributions.<sup>3f,6c</sup> The structures of the MCFs are reminiscent of aerogels (see the TEM section). Aerogels also possess large pores, but the preparation of aerogels<sup>18</sup> is time-consuming, requiring prolonged gel times, solvent exchange, and supercritical drying. Furthermore, aerogels typically possess broad pore size distributions.<sup>18</sup> In comparison to these synthesis methods, the microemulsion templating route is easier, more efficient, and less time-consuming and leads to large mesopores with narrow size distributions.

**X-ray Scattering.** The MCFs have been analyzed using small-angle X-ray scattering (SAXS). X-ray scattering is observed if uniformly sized particles are present, as opposed to X-ray diffraction associated with periodic structures. The SAXS data are desmeared by the direct method.<sup>19</sup> To reduce the SAXS data to coherent scattering arising from the pores and to minimize the contribution from diffuse scattering, a background described by a power law curve of the form  $y = a + b(x - c)^d$  is subtracted and weighted to lie on the desmeared SAXS data for angles  $2\theta > 2^\circ$  and on the local minima for angles  $2\theta \leq 2^\circ$ .<sup>20</sup> Scattering simulations, as described in ref 21 for isotropic polydisperse systems, have been carried out for different types of simple bodies to fit the SAXS data. The X-ray data are in good agreement with simulated scattering from uniform spheres of radius  $R$ , for which the scattering intensity  $I$  is described by  $I(t) = \phi^2(t) = 9((\sin t - t \cos t)/t^3)^2$ , with  $t = sR$  and  $|s| = (4\pi \sin \theta)/\lambda$ .<sup>21</sup> We have also

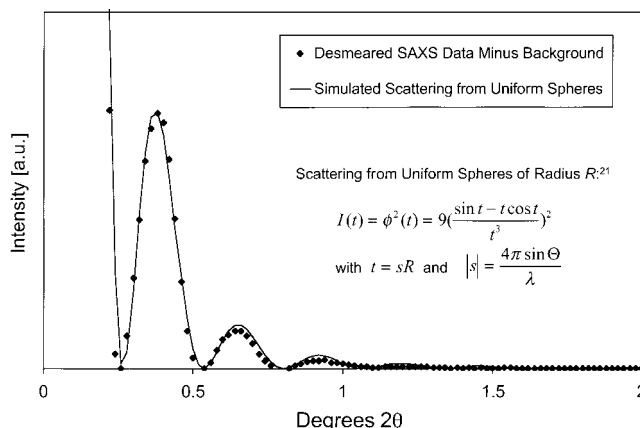


**Figure 1.** Small-angle X-ray scattering (SAXS) pattern of a MCF and corresponding fit based on scattering due to uniform spheres.<sup>21</sup> This MCF was prepared with TMB/P123 = 1.5 in the presence of  $\text{NH}_4\text{F}$  and aged at  $100^\circ\text{C}$ . Please note the occurrence of three higher order peaks that decay exponentially in intensity, which is an indication of the fairly uniformly sized spherical cells.

**Table 1.** Physical Data for MCFs<sup>a</sup>

sample	TMB/P123 (w/w) <sup>b</sup>	$D_s$ (nm) <sup>c</sup>	$D_c$ (nm) <sup>d</sup>	$D_w$ (nm) <sup>d</sup>	surface area (m <sup>2</sup> /g) <sup>e</sup>	pore volume (cm <sup>3</sup> /g) <sup>d</sup>	porosity (%) <sup>d</sup>
No $\text{NH}_4\text{F}$							
MCF 1	0.30	25.6	24.0	9.2	700	1.4	76
MCF 2	0.40	28.2	25.5	10.7	880	2.0	82
MCF 3	0.50	30.8	25.7	10.3	780	1.8	80
MCF 4	0.60	30.0	27.0	9.0	1005	2.3	84
MCF 5	0.75	35.4	31.2	9.8	900	2.3	84
MCF 6	1.00	34.4	33.0	10.7	800	2.0	82
MCF 7	1.25	37.4	34.2	10.7	750	1.9	81
MCF 8	1.50	n/a <sup>f</sup>	36.5	11.5	835	2.3	84
With $\text{NH}_4\text{F}$ <sup>g</sup>							
MCF 1-F	0.30	28.2	28.4	15.5	590	1.9	81
MCF 2-F	0.40	29.2	28.7	16.4	575	1.9	81
MCF 3-F	0.50	29.4	29.8	17.0	560	2.1	82
MCF 4-F	0.60	29.2	28.9	16.5	580	2.0	82
MCF 5-F	0.75	30.0	30.1	16.5	600	2.1	82
MCF 6-F	1.00	32.2	32.2	16.5	625	2.2	83
MCF 7-F	1.25	32.6	33.7	17.5	625	2.3	84
MCF 8-F	1.50	33.6	35.5	17.7	625	2.4	84
MCF 9-F	2.00	36.6	37.6	17.8	605	2.4	84
MCF 10-F	2.50	39.4	42.0	19.1	595	2.3	84

<sup>a</sup> Aging temperature  $100^\circ\text{C}$ . <sup>b</sup> Weight ratio using a fixed amount of P123 (TMB = 1,3,5-trimethylbenzene; P123 = Pluronic surfactant<sup>27</sup>). <sup>c</sup> Sphere diameter,  $D_s$ , determined from small-angle X-ray scattering analyses.<sup>21</sup> <sup>d</sup> Determined from nitrogen sorption measurements.<sup>11</sup> <sup>e</sup> Cell diameter,  $D_c$ , and window diameter,  $D_w$ , determined according to the BdB–FHH method.<sup>9</sup> <sup>f</sup> BET method.<sup>10</sup> <sup>g</sup> Scattering peaks poorly resolved. <sup>h</sup>  $\text{NH}_4\text{F}/\text{Si}$  molar ratio 0.03.

tried to fit the SAXS data to scattering from nonuniform spheres with polydispersities  $\text{PD} \approx 10\%$ ; these simulations, however, give only poor fits of the recorded SAXS data. On the basis of these results, we conclude that the cells in the MCF materials are spherical and quite uniform in size.

Figure 1 shows the recorded SAXS data and the corresponding simulation for MCF 8-F, which is prepared with TMB/P123 = 1.5 in the presence of  $\text{NH}_4\text{F}$  (see Table 1). The scattering pattern is well-resolved and shows one strong primary peak and three higher order peaks with exponentially decreasing intensities. The occurrence of the higher order peaks is an indication of the narrow size distribution of the spherical cells.<sup>21</sup> The sphere diameters  $D_s$ , determined from SAXS simulations, are given in Tables 1–3 for MCFs prepared under

(15) Schacht, S.; Huo, Q.; Voigt-Martin, I. G.; Stucky, G. D.; Schüth, F. *Science* **1996**, *273*, 768.

(16) Huo, Q.; Feng, J.; Schüth, F.; Stucky, G. D. *Chem. Mater.* **1997**, *9*, 14.

(17) (a) Langevin, D. *Acc. Chem. Res.* **1988**, *21*, 255. (b) Huang, J. S. *J. Surface Sci. Technol.* **1989**, *5*, 83. (c) Kabalnov, A.; Lindman, B.; Olsson, U.; Piculell, L.; Thuresson, K.; Wennerström, H. *Colloid Polym. Sci.* **1996**, *274*, 297. (d) Kegel, W. K.; Reiss, H. *Ber. Bunsen-Ges. Phys. Chem.* **1996**, *100*, 300.

(18) For recent reviews, see: (a) Hüsing, N.; Schubert, U. *Angew. Chem., Int. Ed.* **1998**, *37*, 22. (b) Schneider, M.; Baiker, A. *Catal. Rev.-Sci. Eng.* **1995**, *37*, 515.

(19) Singh, M. A.; Ghosh, S. S.; Shannon, R. F. *J. Appl. Crystallogr.* **1993**, *26*, 787.

(20) Mateu, L.; Tardieu, A.; Luzzati, V.; Aggerbeck, L.; Scanu, A. M. *J. Mol. Biol.* **1972**, *70*, 105.

(21) Feigin, L. A.; Svergun, D. I. *Structure Analysis by Small-Angle X-ray and Neutron Scattering*; Plenum Press: New York, 1987.

**Table 2. Physical Data for MCFs Aged at 100 or 120 °C**

sample	TMB/P123 (w/w) <sup>a</sup>	$D_S$ (nm) <sup>b</sup>	$D_C$ (nm) <sup>c</sup>	$D_W$ (nm) <sup>c</sup>	surface area (m <sup>2</sup> /g) <sup>d</sup>	pore volume (cm <sup>3</sup> /g) <sup>e</sup>	porosity (%) <sup>e</sup>
MCF 1 series	0.30	25.6 <sup>e</sup>	24.0 <sup>e</sup>	9.2 <sup>e</sup>	700 <sup>e</sup>	1.4 <sup>e</sup>	76 <sup>e</sup>
		28.0 <sup>f</sup>	25.6 <sup>f</sup>	13.2 <sup>f</sup>	645 <sup>f</sup>	1.8 <sup>f</sup>	80 <sup>f</sup>
MCF 2 series	0.40	28.2 <sup>e</sup>	25.5 <sup>e</sup>	10.7 <sup>e</sup>	880 <sup>e</sup>	2.0 <sup>e</sup>	82 <sup>e</sup>
		29.0 <sup>f</sup>	29.1 <sup>f</sup>	15.5 <sup>f</sup>	710 <sup>f</sup>	2.4 <sup>f</sup>	84 <sup>f</sup>
MCF 3 series	0.50	30.8 <sup>e</sup>	25.7 <sup>e</sup>	10.3 <sup>e</sup>	780 <sup>e</sup>	1.8 <sup>e</sup>	80 <sup>e</sup>
		30.2 <sup>f</sup>	30.1 <sup>f</sup>	15.5 <sup>f</sup>	590 <sup>f</sup>	2.0 <sup>f</sup>	82 <sup>f</sup>
MCF 4 series	0.60	30.0 <sup>e</sup>	27.0 <sup>e</sup>	9.0 <sup>e</sup>	1005 <sup>e</sup>	2.3 <sup>e</sup>	84 <sup>e</sup>
		32.2 <sup>f</sup>	30.4 <sup>f</sup>	13.6 <sup>f</sup>	680 <sup>f</sup>	2.2 <sup>f</sup>	83 <sup>f</sup>

<sup>a</sup> Weight ratio using a fixed amount of P123 (TMB = 1,3,5-trimethylbenzene; P123 = Pluronic surfactant<sup>27</sup>). <sup>b</sup> Sphere diameter,  $D_S$ , determined from small-angle X-ray scattering analyses.<sup>21</sup> <sup>c</sup> Determined from nitrogen sorption. Cell diameter,  $D_C$ , and window diameter,  $D_W$ , determined according to the BdB-FHH method.<sup>9</sup> <sup>d</sup> BET method.<sup>10</sup> <sup>e</sup> Aging temperature 100 °C. <sup>f</sup> Aging temperature 120 °C.

different synthesis conditions. The  $D_S$  values agree with the cell diameters  $D_C$ , derived from nitrogen sorption, and with the cell sizes obtained from transmission electron microscopy (see the TEM section). The  $\text{NH}_4\text{F}$ -treated MCFs exhibit better resolved scattering peaks and show a closer match between the sphere and cell diameters (see Tables 1–3). This may be related to the mineralizing effect of fluoride that leads to improved structural organization and improved X-ray diffraction patterns in zeolites and mesoporous silicas.<sup>4c,31,22</sup> Hydrolysis and condensation of silica are, in principle, reversible in the presence of fluoride.<sup>14</sup> Solution mass transport turned out to be important in the preparation of silica aerogels.<sup>18a</sup> Silica condensed at thermodynamically less favorable regions is redissolved and then condenses at thermodynamically more favorable regions.<sup>18a</sup> Similar effects may take place in the MCFs, especially in the presence of fluoride, thereby giving rise to more homogeneous cells with fewer defects.

**Nitrogen Sorption.** The porosity of the MCFs has been investigated by nitrogen sorption analyses. The isotherms are of type IV and show steep hystereses of type H1 at high relative pressures (see Figure 2), which is typical for mesoporous materials that exhibit capillary condensation and evaporation and have large pore sizes with narrow size distributions.<sup>11</sup> Our modification<sup>9</sup> of the Broekhoff–de Boer<sup>23</sup> (BdB) pore size analysis makes it possible to derive the cell sizes from the adsorption branches of the isotherms, while the desorption branches give the window sizes.<sup>9,11,23</sup> The results from nitrogen sorption, SAXS, and TEM (see below) are in agreement with ink-bottle-type pores, in which large spherical cells (bodies of the ink bottles) are interconnected by narrower windows (bottlenecks).<sup>11</sup> Figure 2 shows typical isotherms and the corresponding BdB-FHH<sup>9</sup> pore size analyses for MCFs that have been prepared under different synthesis conditions with an aging temperature of 100 °C. Figure 2a illustrates the isotherm and pore size distributions of MCF 2 (see Table 1) that is

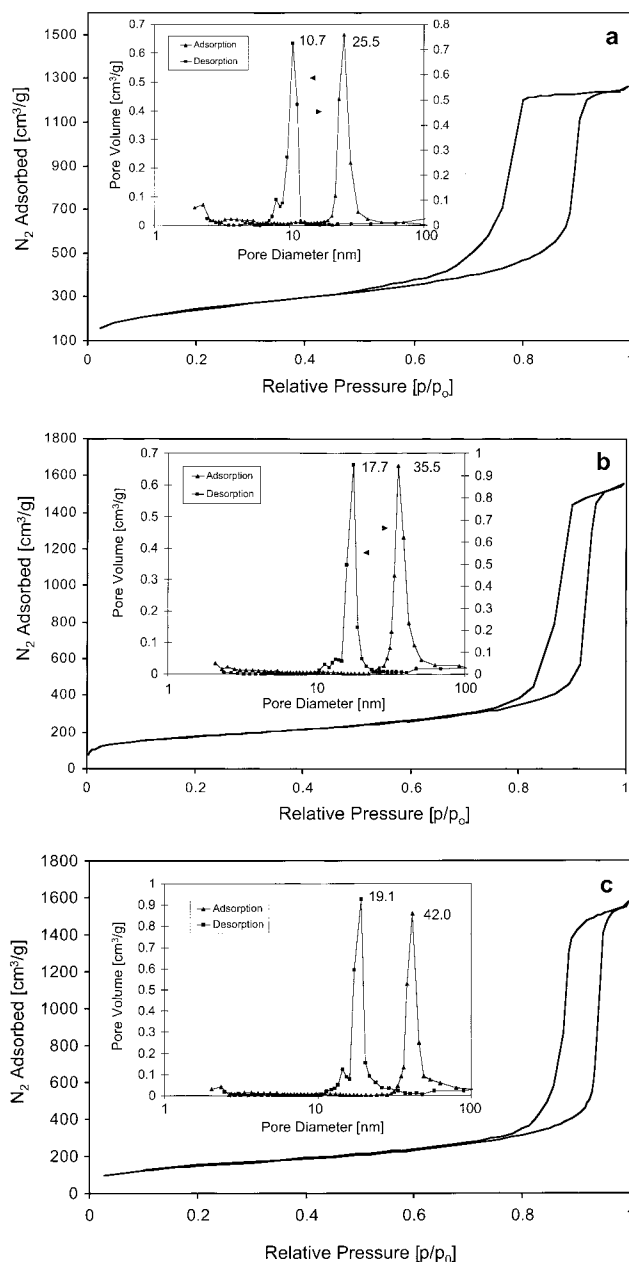


**Figure 2.** Nitrogen sorption isotherms and corresponding pore size analyses for MCFs based on a modified Broekhoff–de Boer method (BdB-FHH):<sup>9</sup> (a) nitrogen isotherm of MCF 2 synthesized with TMB/P123 = 0.4 and aged at 100 °C; (b) nitrogen isotherm of MCF 8-F synthesized with TMB/P123 = 1.5 in the presence of  $\text{NH}_4\text{F}$  and aged at 100 °C; (c) nitrogen isotherm of MCF 10-F synthesized with TMB/P123 = 2.5 in the presence of  $\text{NH}_4\text{F}$  and aged at 100 °C; (insets) BdB-FHH pore size distributions.<sup>9</sup> The isotherms are consistent with ink-bottle-type mesopores in which large fairly uniform cells are interconnected by smaller windows.<sup>11</sup> The sharp peaks in the pore size distribution plots confirm the narrow pore size distributions of both the cells and the windows, and support the findings from the simulations of our SAXS

(22) (a) Guth, J. L.; Kessler, H.; Wey, R. *Stud. Surf. Sci. Catal.* **1986**, *28*, 121. (b) Silva, F. H. P.; Pastore, H. O. *Chem. Commun.* **1996**, 833. (c) Voegtlin, A. C.; Ruch, F.; Guth, J. L.; Patarin, J.; Huve, L. *Microporous Mater.* **1997**, *9*, 95.

(23) (a) Broekhoff, J. C. P.; de Boer, J. H. *J. Catal.* **1967**, *9*, 8. (b) Broekhoff, J. C. P.; de Boer, J. H. *J. Catal.* **1967**, *9*, 15. (c) Broekhoff, J. C. P.; de Boer, J. H. *J. Catal.* **1968**, *10*, 153. (d) Broekhoff, J. C. P.; de Boer, J. H. *J. Catal.* **1968**, *10*, 368. (e) Broekhoff, J. C. P.; de Boer, J. H. *J. Catal.* **1968**, *10*, 377.

prepared with TMB/P123 = 0.4, Figure 2b shows the isotherm and pore size distributions of MCF 8-F prepared in the presence of  $\text{NH}_4\text{F}$  with TMB/P123 = 1.5, and Figure 2c displays the isotherm and pore size distributions of MCF 10-F prepared in the presence of  $\text{NH}_4\text{F}$  with TMB/P123 = 2.5. The sharp peaks in the pore size distribution plots confirm the narrow pore size distributions of both the cells and the windows, and support the findings from the simulations of our SAXS

**Table 3. Physical Data for MCFs Prepared with  $\text{NH}_4\text{F}^a$  and Aged at 100 or 120 °C**

sample	TMB/P123 (w/w) <sup>b</sup>	$D_S$ (nm) <sup>c</sup>	$D_C$ (nm) <sup>d</sup>	$D_W$ (nm) <sup>d</sup>	surface area (m <sup>2</sup> /g) <sup>e</sup>	pore volume (cm <sup>3</sup> /g) <sup>d</sup>	porosity (%) <sup>d</sup>
MCF 1-F series	0.30	28.2 <sup>f</sup>	28.4 <sup>f</sup>	15.5 <sup>f</sup>	590 <sup>f</sup>	1.9 <sup>f</sup>	81 <sup>f</sup>
		31.4 <sup>g</sup>	33.6 <sup>g</sup>	17.3 <sup>g</sup>	440 <sup>g</sup>	1.8 <sup>g</sup>	80 <sup>g</sup>
MCF 2-F series	0.40	29.2 <sup>f</sup>	28.7 <sup>f</sup>	16.4 <sup>f</sup>	575 <sup>f</sup>	1.9 <sup>f</sup>	81 <sup>f</sup>
		31.6 <sup>g</sup>	33.7 <sup>g</sup>	19.1 <sup>g</sup>	445 <sup>g</sup>	2.1 <sup>g</sup>	82 <sup>g</sup>
MCF 3-F series	0.50	29.4 <sup>f</sup>	29.8 <sup>f</sup>	17.0 <sup>f</sup>	560 <sup>f</sup>	2.1 <sup>f</sup>	82 <sup>f</sup>
		33.0 <sup>g</sup>	35.6 <sup>g</sup>	20.6 <sup>g</sup>	410 <sup>g</sup>	2.1 <sup>g</sup>	82 <sup>g</sup>
MCF 4-F series	0.60	29.2 <sup>f</sup>	28.9 <sup>f</sup>	16.5 <sup>f</sup>	580 <sup>f</sup>	2.0 <sup>f</sup>	82 <sup>f</sup>
		33.8 <sup>g</sup>	38.4 <sup>g</sup>	18.6 <sup>g</sup>	445 <sup>g</sup>	2.1 <sup>g</sup>	82 <sup>g</sup>
MCF 5-F series	0.75	30.0 <sup>f</sup>	30.1 <sup>f</sup>	16.5 <sup>f</sup>	600 <sup>f</sup>	2.1 <sup>f</sup>	82 <sup>f</sup>
		32.4 <sup>g</sup>	33.7 <sup>g</sup>	17.5 <sup>g</sup>	455 <sup>g</sup>	2.1 <sup>g</sup>	82 <sup>g</sup>
MCF 6-F series	1.00	32.2 <sup>f</sup>	32.2 <sup>f</sup>	16.5 <sup>f</sup>	625 <sup>f</sup>	2.2 <sup>f</sup>	83 <sup>f</sup>
		33.2 <sup>g</sup>	35.9 <sup>g</sup>	19.2 <sup>g</sup>	435 <sup>g</sup>	2.1 <sup>g</sup>	82 <sup>g</sup>
MCF 7-F series	1.25	32.6 <sup>f</sup>	33.7 <sup>f</sup>	17.5 <sup>f</sup>	625 <sup>f</sup>	2.3 <sup>f</sup>	84 <sup>f</sup>
		34.2 <sup>g</sup>	36.2 <sup>g</sup>	20.8 <sup>g</sup>	450 <sup>g</sup>	2.4 <sup>g</sup>	84 <sup>g</sup>
MCF 8-F series	1.50	33.6 <sup>f</sup>	35.5 <sup>f</sup>	17.7 <sup>f</sup>	625 <sup>f</sup>	2.4 <sup>f</sup>	84 <sup>f</sup>
		40.4 <sup>g</sup>	39.9 <sup>g</sup>	22.5 <sup>g</sup>	445 <sup>g</sup>	2.4 <sup>g</sup>	84 <sup>g</sup>

<sup>a</sup>  $\text{NH}_4\text{F}/\text{Si}$  molar ratio 0.03. <sup>b</sup> Weight ratio using a fixed amount of P123 (TMB = 1,3,5-trimethylbenzene; P123 = Pluronic surfactant<sup>27</sup>). <sup>c</sup> Sphere diameter,  $D_S$ , determined from small-angle X-ray scattering analyses.<sup>21</sup> <sup>d</sup> Determined from nitrogen sorption. Cell diameter,  $D_C$ , and window diameter,  $D_W$ , determined according to the BdB-FHH method.<sup>9</sup> <sup>e</sup> BET method.<sup>10</sup> <sup>f</sup> Aging temperature 100 °C. <sup>g</sup> Aging temperature 120 °C.

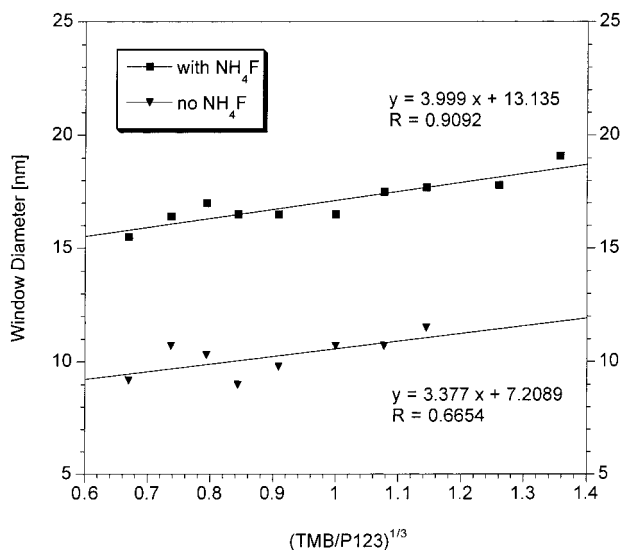


**Figure 3.** Control of the window sizes in MCFs (aged at 100 °C) by  $\text{NH}_4\text{F}$  addition and as a function of the cube root of the TMB concentration that is expressed in terms of the TMB/P123 weight ratio. Adding small amounts of  $\text{NH}_4\text{F}$  ( $\text{NH}_4\text{F}/\text{Si}$  molar ratio 0.03) to the MCF synthesis mixtures selectively increases the window sizes by 50–80%. The window sizes also increase with the TMB concentration.

data. Both the adsorption and desorption branches of the isotherms are shifted toward larger relative pressures ( $p/p_0$ ) in the cases of MCF 8-F and MCF 10-F, suggesting that the cell sizes and window sizes are larger in MCF 8-F and MCF 10-F than in MCF 2. The BdB-FHH pore size analyses corroborate this qualitative interpretation of the isotherms (see insets in Figure 2 and Table 1). By increasing TMB/P123 from 0.4 (Figure 2a) to 1.5 (Figure 2b), the cell size increases from 26 to 36 nm (~40%), while the window size increases from 11 to 18 nm (~64%). To separate the effects of TMB concentration and  $\text{NH}_4\text{F}$  addition on the pores, we have prepared MCFs with varying amounts of TMB both with and without  $\text{NH}_4\text{F}$  addition. These data are summarized in Table 1. Only ~7% of the observed ~64% increase in window size (Figure 2b vs Figure 2a) is due to the higher TMB concentration. The remaining ~57% is due to the presence of  $\text{NH}_4\text{F}$ . From the window diameter  $D_W$  values

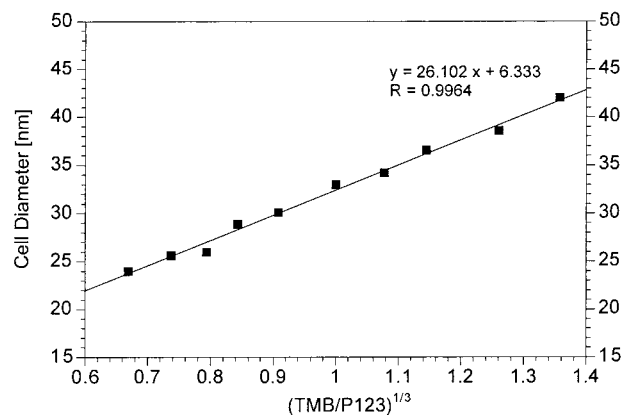


**Figure 4.** Correlation of the cell sizes of MCFs prepared with and without  $\text{NH}_4\text{F}$  addition as a function of the cube root of the concentration of TMB (aging temperature 100 °C). The TMB concentration is expressed in terms of the TMB/P123 weight ratio. The cell sizes increase linearly with the cube root of the TMB concentration, which is in agreement with a spherical model for both the templating TMB/P123 droplets and the cells ( $V_{\text{sphere}} = 4/3\pi R^3$ ). The cell diameter can be adjusted by adding the appropriate amount of TMB.

in Table 1, it is evident that adding  $\text{NH}_4\text{F}$ , at a  $\text{NH}_4\text{F}/\text{Si}$  molar ratio of 0.03, enlarges the sizes of the windows by ~50–80%. Comparison of the sphere diameters  $D_S$  and the cell diameters  $D_C$  in Table 1 for MCF samples prepared with and without  $\text{NH}_4\text{F}$  indicates that  $\text{NH}_4\text{F}$  does not appreciably affect the size of the cells, whereas the size of the windows is substantially modified. The effect of  $\text{NH}_4\text{F}$  addition on the window diameters is displayed in Figure 3. The window sizes seem to increase with increasing TMB concentration; however, there is a fair amount of scatter in the data. In contrast, the cell sizes increase linearly with the cube root of the TMB concentration, as shown in Figure 4. This behavior is expected for spherical cells of radius  $R$  with volume  $V = 4/3\pi R^3$ . A similar linear relationship is observed for the microemulsion droplets used to template the MCFs.<sup>8</sup>

The BET<sup>10</sup> surface areas (see Tables 1–3) are 590–1005 m<sup>2</sup>/g for MCFs prepared without  $\text{NH}_4\text{F}$  and 410–625 m<sup>2</sup>/g for  $\text{NH}_4\text{F}$ -treated MCFs, depending upon the aging temperature (see below). The reduced surface

areas for  $\text{NH}_4\text{F}$ -treated MCFs may be related to the increased window sizes in these materials. As the windows become larger, they take away more of the cell's surface area (see Figure 6). Also, more dense framework walls may contribute to the decreased surface areas. Support for this hypothesis is provided by  $^{29}\text{Si}$  MAS NMR experiments of calcined MCFs, where the  $Q^3/Q^4$  ratios for  $\text{NH}_4\text{F}$ -treated MCFs ( $Q^3/Q^4 = 0.40$ ) are smaller than for MCFs synthesized without fluoride addition ( $Q^3/Q^4 = 0.45$ ). This indicates that the framework walls are more dense in the case of the fluoride-treated MCFs, which is in agreement with the determined surface areas. The pore volumes and porosities of the MCFs are listed in Tables 1–3. For MCFs prepared with  $\text{NH}_4\text{F}$ , the pore volumes (1.8–2.4  $\text{cm}^3/\text{g}$ ) and the porosities (80–84%) increase with the TMB concentration. Similar trends are observed for the MCFs prepared without  $\text{NH}_4\text{F}$ , which have pore volumes of 1.4–2.4  $\text{cm}^3/\text{g}$  and porosities of 76–84%, but the data show some scatter in this case. We also note that the pore volumes and porosities increase with the aging temperature (see below) for both types of MCF materials, as reflected by the data presented in Tables 2 and 3.

**Transmission Electron Microscopy.** Figure 5 shows a collection of representative TEM images of MCFs synthesized under different conditions. All samples possess a disordered array of silica struts, which is the characteristic structural feature of the MCFs.<sup>7</sup> A schematic of the strutlike structure, given in Figure 6, shows the cells of the MCF structure framed by the silica struts. This strutlike structure of MCFs is reminiscent of aerogels.<sup>18</sup> TEM analyses indicate that the phase transition<sup>24</sup> from the undulated SBA-15-type, ordered structure with  $p6mm$  symmetry to the strutlike MCF structure occurs at  $\text{TMB}/\text{P123} = 0.2\text{--}0.3$  if  $\text{NH}_4\text{F}$  is present ( $\text{NH}_4\text{F}/\text{Si}$  molar ratio 0.03), just as in the absence of  $\text{NH}_4\text{F}$ .<sup>24</sup>

Both X-ray scattering and nitrogen sorption experiments suggest that the MCFs possess uniform spherical cells, which is further verified by TEM analyses. The cell sizes estimated from TEM are consistent with the sphere and cell sizes determined from X-ray scattering ( $D_S$ ) and nitrogen sorption ( $D_C$ ) summarized in Table 1. In the case of MCF 2, the TEM pore size is 26–28 nm,  $D_S = 28$  nm,  $D_C = 26$  nm, for MCF 5, the TEM pore size is ~29–34 nm (higher magnification image),  $D_S = 35$  nm,  $D_C = 31$  nm, and for MCF 8-F, the TEM pore size is ~33 nm,  $D_S = 34$  nm,  $D_C = 36$  nm. Slight deformations of the spherical cells can be seen in the higher magnification TEM images in Figure 5b,d. Such distortions may be caused by the nonperfect packing of the spherical, colloidal particles (as discussed below) due to their slight polydispersity. The empty voids inevitably formed between nonperfectly packed spheres must be filled for energetic reasons, which may be accomplished by slight deformations of the spherical cells.

The wall thickness of the MCFs is estimated by TEM to be ~4–6 nm, in agreement with the thick, robust framework walls observed in acid-synthesized SBA-15-type mesoporous silica.<sup>3c,d,1</sup> The thick walls may explain why the MCFs withstand normal drying and calcination

without collapse of the mesostructure due to capillary forces. In contrast, aerogels must be subjected to supercritical drying techniques to prevent collapse of the structure and substantial shrinking.<sup>18</sup> We are unable to image the windows connecting the cells in the MCFs, probably due to the smaller window sizes and the poor contrast among cells, windows, and the silica framework.

**Scanning Electron Microscopy.** The morphologies of representative MCFs are illustrated in the SEM images in Figure 7. Slight morphological differences can be detected for the MCF materials prepared with and without  $\text{NH}_4\text{F}$  addition, whereas different TMB concentrations do not seem to affect the particle morphologies. The MCFs synthesized without  $\text{NH}_4\text{F}$  exhibit a cauliflower-type morphology (Figure 7, top panel), whereas the  $\text{NH}_4\text{F}$ -treated MCFs show a coral-type morphology (Figure 7, bottom panel). For both types of MCFs, elongated particles measuring ~40  $\mu\text{m}$  in length and ~15  $\mu\text{m}$  in width are obtained.

**Thermal Analysis.** The MCFs have been subjected to simultaneous thermogravimetric and differential thermal analyses (TGA/DTA). The results are very similar to those of SBA-15-type mesoporous silicas.<sup>3c,d,1</sup> The total weight loss of precalcined MCFs is ~60%. The TGA/DTA data show two processes: a 10% weight loss at 50–100  $^\circ\text{C}$  due to the desorption of water and a 50% weight loss from 160 to 240  $^\circ\text{C}$ . The second weight loss, which is accompanied by a strong exothermic DTA peak centered at 185  $^\circ\text{C}$ , is due to the decomposition of P123 and other organics. For the evaporation of TMB, we would expect an endothermic peak at 162–164  $^\circ\text{C}$  (the boiling point of TMB); however, this endothermic peak may be masked by the strong exothermic peak from P123 decomposition that begins at 160  $^\circ\text{C}$  as determined in a TGA/DTA control experiment with bulk P123. The results from TGA/DTA demonstrate that P123 and TMB are readily removed from the MCFs under mild conditions.

**Aging.** The aging step appears to be important for the formation of MCFs with well-defined pores. When the synthesis is stopped after 24 h at 37–40  $^\circ\text{C}$  without subsequent aging at 100 or 120  $^\circ\text{C}$ , the resulting MCFs have broad and ill-defined  $\text{BdB-FHH}^9$  pore size distributions for the cells. Also, the cell sizes are considerably smaller than those for the aged samples; the window sizes are then limited to 4.8 nm, even if  $\text{NH}_4\text{F}$  has been added. This is in marked contrast to the MCFs aged at 100 and 120  $^\circ\text{C}$ , which have well-defined, large mesopores with narrow size distributions. We believe that agglomeration and packing of the composite droplets occur during aging at higher temperatures and are essential for the formation of MCFs with well-defined pores. The polydispersity of the microemulsion templates varies from 11% to 21%,<sup>8</sup> which is typical for microemulsions. However, the results of our X-ray and nitrogen sorption experiments suggest that the pores in the final MCF materials are uniform in size and shape, with size distributions of approximately  $\leq 10\%$ . The narrow pore size distributions may arise from repulsive sphere–sphere interactions between the still flexible composite droplets during packing, which may narrow the potential energy curves of the droplets at the early aging stages of the MCF syntheses. The

(24) Han, Y. J.; Lettow, J. S.; Schmidt-Winkel, P.; Yang, P.; Butler, A.; Stucky, G. D.; Ying, J. Y. Submitted for publication.

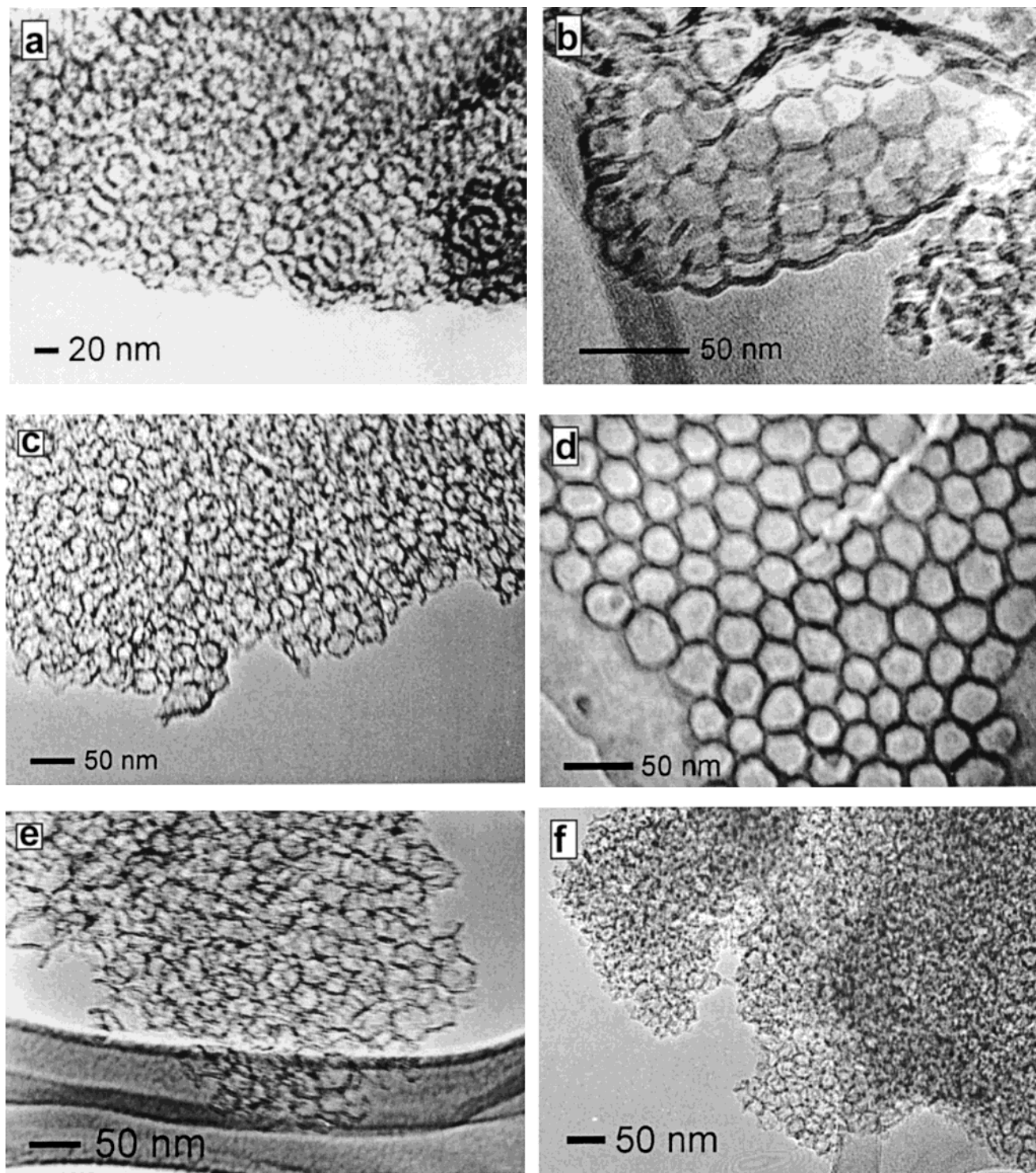


**Figure 5.** TEM images of MCFs prepared under different synthesis conditions reflecting the strutlike structure that is reminiscent of aerogels: (a) MCF 1-F prepared with TMB/P123 = 0.3 in the presence of  $\text{NH}_4\text{F}$ , TEM cell size  $\sim 25$  nm; (b) MCF 2 prepared with TMB/P123 = 0.4, TEM cell size  $\sim 26$ – $28$  nm; (c) MCF 5 prepared with TMB/P123 = 0.75, TEM cell size  $\sim 30$  nm; (d) higher magnification image of MCF 5 prepared with TMB/P123 = 0.75, TEM cell size  $\sim 29$ – $34$  nm; (e) MCF 8 prepared with TMB/P123 = 1.5, TEM cell size  $\sim 35$  nm; (f) MCF 8-F prepared with TMB/P123 = 1.5 in the presence of  $\text{NH}_4\text{F}$ , TEM cell size  $\sim 33$  nm. Wall thickness estimate  $\sim 4$ – $6$  nm.

narrowed size distributions may then be locked in during further aging and condensation to yield MCFs with uniform pores.

The effect of the aging temperature on the pore structure and surface areas of the MCFs is illustrated in Tables 2 and 3. Increasing the aging temperature from 100 to 120 °C enlarges both the cells and windows, increases the pore volumes and porosity, but decreases

the BET surface areas. These trends are observed for MCFs prepared with and without  $\text{NH}_4\text{F}$  addition. In Figure 8, the sizes of the cells and windows are plotted as functions of the cube root of the TMB concentration and aging temperature. We believe that the enlarged pores are related to the temperature sensitivity of the microemulsion droplet sizes.<sup>8</sup> The higher the temperature, the larger the size of the oil droplets<sup>8</sup> that comprise

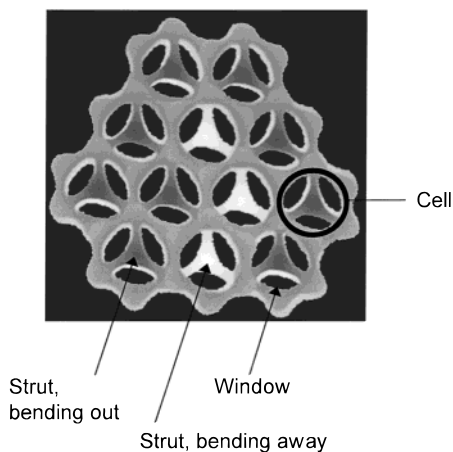


**Figure 6.** Schematic cross section of the strutlike structure exhibited by MCFs. The gray-shaded areas represent the silica framework and the struts (see left arrow), the circular arrays within the cells (see right arrows) represent the windows. The windows are drawn smaller than their actual size for the purpose of clarity. If the windows increase in size, they occupy a larger area of the surface of the cells. Consequently, the struts become thinner and the surface area of the materials is reduced.

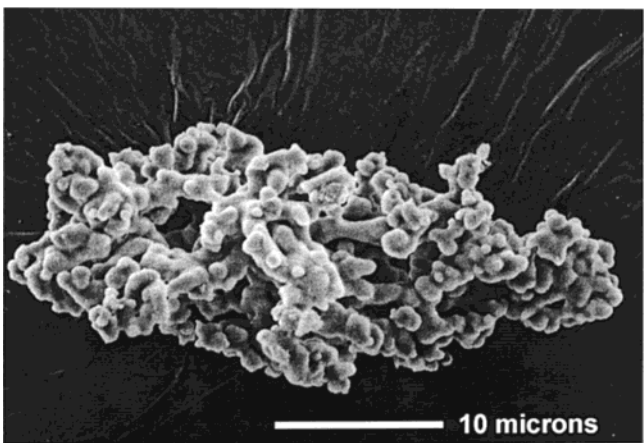
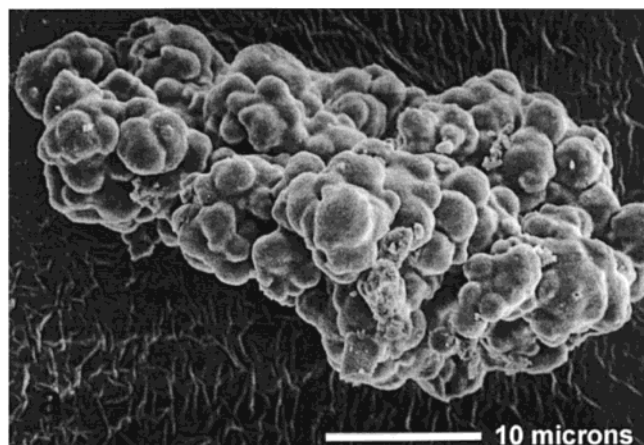


**Figure 7.** Representative SEM images of MCFs. The cauliflower-type morphology of MCFs prepared in the absence of  $\text{NH}_4\text{F}$  is shown in the top panel, and the coral-type morphology of  $\text{NH}_4\text{F}$ -treated MCFs is displayed in the bottom panel.

the hydrophobic volumes around which the silica precursors are proposed to polymerize.<sup>7</sup> We note that the wet composite materials (consisting of organic template, solvent, and silica) isolated after 24 h of stirring at 37–

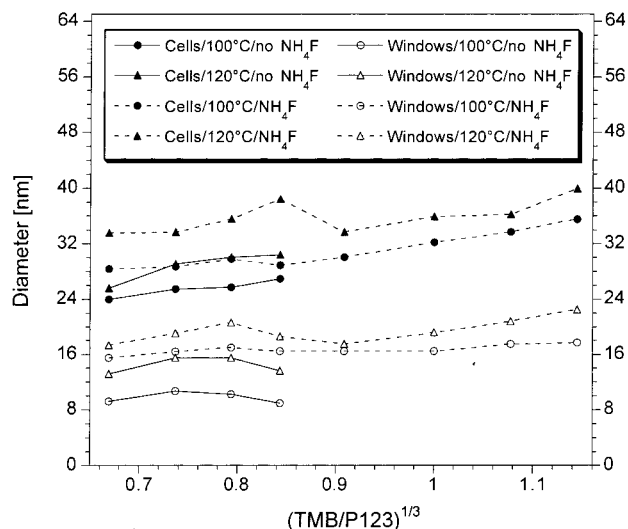


**Figure 8.** Effect of the aging temperature (100 and 120 °C) upon the sizes of the cells and windows of MCFs. The data are derived from nitrogen sorption measurements. The sizes of the windows and the cells are larger if aged at 120 °C for MCFs prepared in both the absence of and in the presence of  $\text{NH}_4\text{F}$ .

40 °C are still flexible, and they rigidify slowly either by drying or during subsequent aging steps at elevated temperatures. Therefore, it is not unreasonable to assume that the “soft silica”-coated TMB/P123 micro-emulsion droplets (composite droplets) increase in size upon exposure to heat, expanding the pore size in the composite material during aging. At the same time, condensation of silica is likely to continue, and the composite material with increased pore size gradually rigidifies. Comparison of the data presented in Tables 2 and 3 and plotted in Figure 8 suggests that an aging temperature of 100 °C gives better control over the cell and window sizes compared to 120 °C, where the scatter of the data is larger.

The reduction of the BET surface areas with increased aging temperature may be related to the enlarged window sizes and more dense framework walls. As the windows become bigger during aging, they take away more of the cells’ surface area. A higher aging temperature increases the degree of silica condensation and thus leads to denser walls. The pore volumes and the porosities increase with higher aging temperature, which can be attributed to the expansions in cell and window sizes.

**Hydrothermal Treatment.** A limitation in the application of MCM-41-type mesoporous materials arises from their instability in hot water.<sup>25</sup> The SBA-15 family of mesoporous silicas exhibits enhanced long-range order and no observable structural decomposition after 48 h or more in water at 100 °C, without postsynthesis treatment for framework stabilization.<sup>3c,d,1</sup> The recently reported MSU-G silicas with nanometer-thick framework walls withstand boiling water for 150 h.<sup>26</sup>

(25) (a) Beck, J. C.; Chu, C. T.; Johanson, I. D.; Kresge, C. T.; Leonowicz, M. E.; Roth, W. J.; Vartuli, J. C.; McCullen, S. B. U.S. Patent 5156829, 1993. (b) Kim, J. M.; Kwak, J. H.; Jim, S.; Ryoo, R. *J. Phys. Chem.* **1995**, *99*, 16742. (c) Ryoo, R.; Kim, J. M.; Ko, C. H.; Shin, C. H. *J. Phys. Chem.* **1996**, *100*, 17718. (d) Ryoo, R.; Kim, J. M.; Shin, C. H.; Lee, J. Y. *Stud. Surf. Sci. Catal.* **1997**, *105*, 45.

(26) Kim, S. S.; Zhang, W.; Pinnavaia, T. J. *Science* **1998**, *282*, 1302.

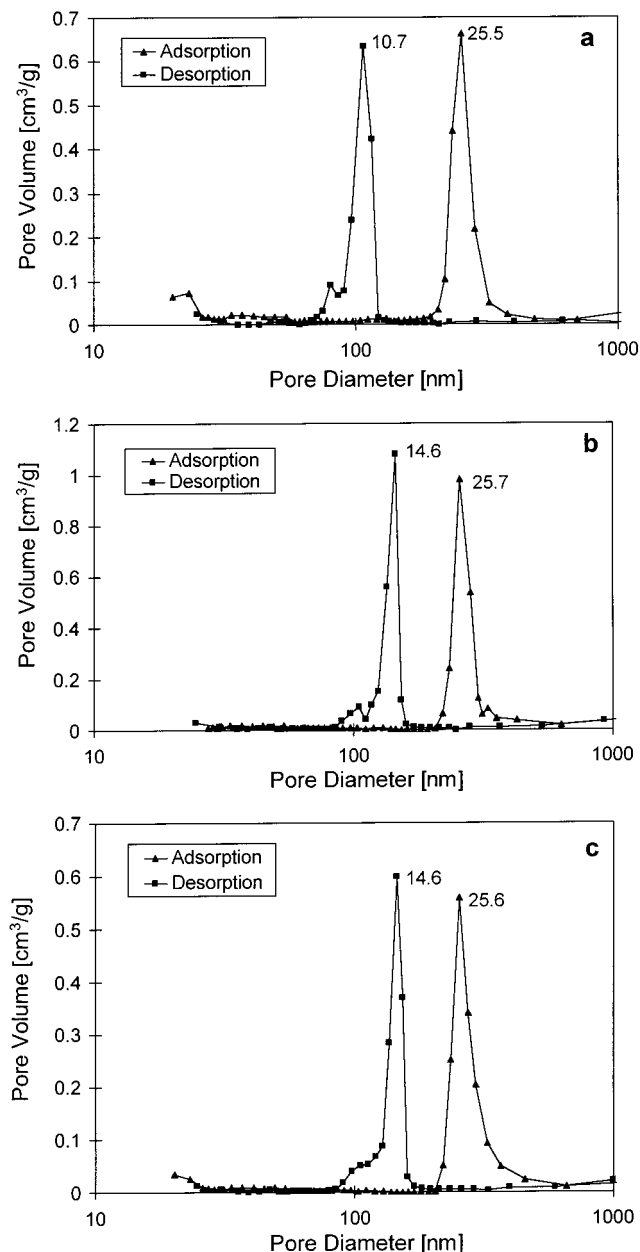


**Figure 9.** Effect of hydrothermal treatment of calcined MCFs in water at 100 °C. This figure shows the pore size distributions for MCF 2 that is hydrothermally treated for (a) 0 h, (b) 24 h, and (c) 65 h. The window size increases from 10.7 to 14.6 nm after 24 h in water at 100 °C. Additional heating, up to at least 65 h, does not change the window size anymore. The size of the cells is not affected by exposure to hot water for at least 65 h. Similar results are obtained for other MCFs.

The MCFs calcined at 500 °C are surprisingly stable with respect to hydrothermal treatment in water at 100 °C, as verified by nitrogen sorption, TEM, and X-ray scattering experiments. The cell sizes and the narrow cell and window size distributions of MCFs prepared without  $\text{NH}_4\text{F}$  remain unchanged during heating in water at 100 °C for at least 65 h. The window sizes increase by ~35–40% during the first 24 h of heating in water; however, no additional enlargement occurs upon further hydrothermal treatment (see Figure 9). The BET surface areas are reduced during hydrothermal treatment. For example, the BET surface area of MCF 2 is reduced from 880 to 525  $\text{m}^2/\text{g}$  after heating in water at 100 °C for 65 h.

The MCFs prepared with  $\text{NH}_4\text{F}$  are more easily restructured than the MCFs prepared without  $\text{NH}_4\text{F}$ . After treatment in boiling water for 24 h, the cells and the windows are enlarged by 10–15% and 15–20%, respectively; however, the widths of the pore size distributions remain narrow. We attribute the difference in restructuring to the presence of minute amounts of fluoride in the calcined,  $\text{NH}_4\text{F}$ -treated MCFs.<sup>31</sup> Because the condensation of silica is reversible in the presence of fluoride,<sup>14</sup> the silica framework of  $\text{NH}_4\text{F}$ -treated MCFs may gradually undergo topotactic reorganization upon heating in water at 100 °C, leading to enlarged pore sizes.

The effects of heating in water can be exploited and used synthetically to selectively increase the window sizes in MCFs. Hydrothermal treatment is therefore a useful alternative to  $\text{NH}_4\text{F}$  addition for window size control if hydrothermally stable MCFs are the targeted materials.

**Amount of TMB.** In our studies, we have systematically varied the amounts of TMB added to the P123 solutions to control the pore sizes in the MCFs. Using a fixed amount of P123, the TMB/P123 weight ratio has been varied from 0 to 2.5. Adding a sufficiently large amount of TMB leads to a phase transformation<sup>24</sup> from the highly ordered  $p6mm$  mesostructure of SBA-15-type mesoporous silicas<sup>3c,d,1</sup> to disordered MCFs.<sup>7</sup> SBA-15-type silicas are obtained at  $\text{TMB}/\text{P123} < 0.2$ , mixed-phase silica consisting of domains of SBA-15 and MCF is found at  $\text{TMB}/\text{P123} = 0.2\text{--}0.3$ , and MCFs are synthesized with  $\text{TMB}/\text{P123} > 0.3$ .<sup>24</sup> From small-angle neutron scattering studies on the microemulsion templates,<sup>8</sup> we know that P123 forms spherical micelles in aqueous solutions at concentrations of ~2.5 wt %, which is in agreement with literature data.<sup>27</sup> We propose that a siliceous liquid crystal (SLC) phase<sup>28</sup> with  $p6mm$  symmetry may form upon addition of TEOS to the P123 surfactant solution.<sup>24</sup> This SLC phase may template the formation of SBA-15-type silicas.<sup>3c,d,1</sup> A similar behavior is described for the formation of MCM-41-type silicas, where the existence of preformed micellar arrays that mimic the final pore structure is not essential for the preparation of highly ordered mesoporous silica.<sup>29</sup> The presence of small amounts of TMB ( $\text{TMB}/\text{P123} < 0.2$ ) may lead to periodic undulations in the one-dimensional cylinders of the SLCs with  $p6mm$  symmetry (presumably formed upon TEOS addition) and may give rise to SBA-15-type, hexagonal silicas with pore sizes of <15–17 nm.<sup>24</sup> Increasing the amount of TMB enhances the undulations in the SLC cylinders, which may no longer be stable at  $\text{TMB}/\text{P123} = 0.3$ . At this point, microemulsion templating takes over, and spherical, TMB-swollen P123 micelles<sup>8</sup> template the formation of the MCFs.<sup>7</sup>

(27) (a) For a comprehensive review, see: (a) Alexandridis, P.; Hatton, T. A. *Colloids Surfaces A: Physicochem. Eng. Aspects* **1995**, *96*, 1. (b) Nace, V. M. In *Nonionic Surfactants, Polyoxyalkylene Block Copolymers*; Nace, V. M., Ed.; Surfactant Science Series; Marcel Dekker: New York, 1996; Vol. 60, pp 145. (c) Pluronic and Tetronic Surfactants, Technical Brochure, BASF Corp., Parsippany, NJ, 1989. (d) Wanka, G.; Hoffmann, H.; Ulbricht, W. *Macromolecules* **1994**, *27*, 4145.

(28) Firouzi, A.; Kumar, D.; Bull, L. M.; Besier, T.; Sieger, P.; Huo, Q.; Walker, S. A.; Zasadzinski, J. A.; Glinka, C.; Nicol, J.; Margolese, D.; Stucky, G. D.; Chmelka, B. F. *Science* **1995**, *267*, 1138.

(29) Glinka, C. J.; Nicol, J. M.; Stucky, G. D.; Ramli, E.; Margolese, D.; Huo, Q.; Higgins, J. B.; Leonowicz, M. E. *J. Porous Mater.* **1996**, *3*, 93.

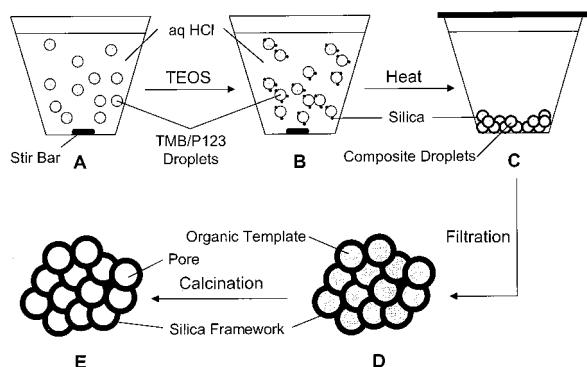


**Figure 10.** Schematic of the suggested stages of the MCF formation: (A) agitated oil-in-water microemulsion consisting of HCl, P123, and TMB; (B) hydrophobic TEOS hydrolyzes at the organic-inorganic interface at the surface of the oil droplets; hydrophilic silica species begin to condense around the oil droplets; (C) during aging at elevated temperature, the silica-coated composite droplets agglomerate and pack while condensation of the silica species continues; this leads to precipitation; (D) as-made composite material where the organic template fills the pores; (E) calcined MCF with open pores.

The concentration of TMB plays the major role in determining the ultimate structures of the mesoporous silicas obtained from P123/TMB templates.<sup>24</sup> For  $0.3 < \text{TMB/P123} \leq 2.5$ , the size of the spherical cells can be controlled continuously from 24 to 42 nm by adjusting the amount of TMB added (see Figure 4).

**Formation of MCFs.** We have recently shown with small-angle neutron scattering that mixing aqueous HCl, P123, and TMB leads to the formation of oil-in-water microemulsions, in which the TMB/P123 droplet size can be controlled by the TMB concentration for use in templating the MCF materials.<sup>8</sup> On this basis, we suggest the following stages for the formation of MCFs, which are schematically illustrated in Figure 10: The MCF synthesis begins with an oil-in-water microemulsion consisting of P123-coated TMB droplets in aqueous HCl.<sup>8</sup> To this system is added hydrophobic TEOS, which hydrolyzes at the surface of the TMB/P123 droplets to form hydrophilic cationic silica species and ethanol (which acts as a cosurfactant).<sup>8</sup> The cationic silica species may begin to condense and form a "soft" silica coating through hydrogen bonding to the P123-coated TMB droplets around the hydrophobic templates to give composite droplets. During aging at elevated temperatures in an autoclave, agglomeration and packing of the composite droplets may occur while the cationic silica species continue to condense. The precipitated aggregates of composite droplets are filtered, dried, and calcined to burn off the organic templates, thus producing the porous MCF material.

We are currently investigating the dynamic evolution of the MCFs by means of in situ small-angle neutron scattering of the microemulsions in the presence of TEOS to learn more about the mechanism of formation of these novel materials.

**Formation of Windows.** The windows interconnecting the cells in the MCFs may form at regions where neighboring composite droplets come into close contact and touch each other. During the polymerization of silica, the hydrophilic poly(ethylene oxide) chains must be expelled from the developing inorganic network, and

may be enriched at certain areas of the composite droplets. These areas are likely to become the contact areas between the composite droplets and may ultimately form the windows between the cells. The increase in the window sizes with increasing aging temperatures may be related to the enlarged droplet sizes and the smaller droplet curvatures that provide a larger contact area between touching spheres.

The silica walls immediately adjacent to the windows are most likely thinner than those for the rest of the cells on the basis of the proposed sphere-touching mechanism of formation. The adsorption and TEM data suggest thick silica walls elsewhere. Since silica hydrolysis and condensation are reversible in the presence of fluoride,<sup>14</sup> it is reasonable to assume that fluoride may catalyze<sup>30</sup> the partial dissolution of silica at these thin regions around the windows, and may thereby increase the window sizes. This view is supported by our observation that the window sizes of calcined MCFs can be selectively enlarged by hydrothermal treatment in water at 100 °C (see Figure 9). Solution mass transport is important in the formation of aerogels<sup>18a</sup> and zeolites;<sup>31</sup> material is dissolved from thermodynamically unfavorable regions and condenses at thermodynamically more favorable regions.<sup>18a</sup> Similar phenomena may take place in MCFs and may account for the enlarged window sizes in response to increased aging temperature, to hydrothermal treatment, and to  $\text{NH}_4\text{F}$  addition.

**Amount of  $\text{NH}_4\text{F}$ .** We have found that it is not possible to selectively enlarge the window sizes beyond the values reported in Tables 1 and 3 by increasing the amount of added  $\text{NH}_4\text{F}$ . Increasing the  $\text{NH}_4\text{F/Si}$  molar ratio from 0.03 to 0.06 leads to immediate gelling of the MCF synthesis mixtures upon TEOS addition, and amorphous gels are produced instead of MCFs. Decreasing the  $\text{NH}_4\text{F/Si}$  molar ratio to 0.008 does not seem to affect the MCFs appreciably. These findings agree with our previous studies on the effects of  $\text{NH}_4\text{F}$  on acid-synthesized SBA-15-type mesoporous silicas, where a  $\text{NH}_4\text{F/Si}$  molar ratio of 0.03 produces excellent mesostructures.<sup>31</sup>

**Addition of TEOS.** The concentration of TEOS influences the quality of the MCFs; similar behavior is observed for SBA-15-type silicas.<sup>3d</sup> The amount of TEOS is expressed in terms of the TEOS/TEOS\* weight ratio, where TEOS\* is the standard amount of 4.4 g used for the MCF syntheses. We have investigated MCFs prepared with various amounts of TEOS, corresponding to TEOS/TEOS\* = 1.25, 1.50, 1.75, and 2.00 for different TMB concentrations in the presence and in the absence of  $\text{NH}_4\text{F}$ , while all the other synthesis conditions remained unchanged. The quality of the X-ray scattering patterns is already considerably reduced for TEOS/TEOS\* = 1.25, and deteriorates further at increased TEOS concentrations. The pore size distributions become broadened and ill-defined for TEOS/TEOS\*  $\geq 1.25$ . Even if the amount of added  $\text{NH}_4\text{F}$  is raised commensurate with the increased concentration of TEOS to maintain the  $\text{NH}_4\text{F/Si}$  molar ratio of 0.03, the quality of the MCFs is poor compared to that produced with the standard TEOS concentration.

(30) (a) Pope, E. J. A.; Mackenzie, J. D. *J. Non-Cryst. Solids* **1986**, *87*, 185. (b) Brinker, C. J. *J. Non-Cryst. Solids* **1988**, *100*, 31.

(31) Mintova, S.; Olson, N. H.; Valtchev, V.; Bein, T. *Science* **1999**, *283*, 958.

We have varied the time intervals between the introduction of TMB and the addition of TEOS to investigate if it is possible to influence the structure and properties of the MCFs<sup>24</sup> by allowing for different interaction times between TMB and P123 prior to TEOS addition. Varying this time interval from 0, 5, 15, 25, 35, 45, 55, to 65 min has no effect on the MCFs produced. The solid materials isolated are very similar and exhibit no appreciable differences, as evidenced by X-ray scattering, nitrogen sorption, and TEM.

The MCFs are templated by microemulsion droplets,<sup>8</sup> and microemulsions are thermodynamically stable systems that form spontaneously upon mixing water, surfactant, and oil.<sup>17</sup> We believe that the microemulsions form immediately upon adding sufficient amounts of TMB (TMB/P123 > 0.3<sup>24</sup>) to the P123 solutions, and are hence immediately available to template the MCFs. From our studies on the MCF and SBA-15-type<sup>3c,d,l</sup> materials, we have learned that the sequence of adding the different reagents is critical for the formation of MCFs with well-defined, uniform pores, but the time intervals between the different additions seem to play a negligible role.

### Conclusions

We have synthesized mesostructured cellular foams as a new class of three-dimensional hydrothermally robust materials with ultralarge mesopores by using microemulsion templates. The novel MCF materials are reminiscent of aerogels and are composed of uniform spherical cells whose size can be controlled by the

amount of organic oil added. The cells are interconnected by windows with a narrow size distribution. The windows can be selectively enlarged by adding small amounts of NH<sub>4</sub>F, or by postsynthesis hydrothermal treatment in water. The pore sizes, BET surface areas, and pore volumes can be controlled by the aging temperature.

The well-defined, adjustable, ultralarge pores of MCFs and the simple microemulsion templating synthesis described in this work present new possibilities to engineer mesoporous systems for applications such as catalyst supports where mass transport is often limited by small pore openings.

**Acknowledgment.** Funding for these studies was provided by the National Science Foundation under Grant No. DMR-9634396, the Materials Research Laboratory program of the National Science Foundation under Award No. DMR-9632716, the U.S. Army Research Office under Grant No. DAAH 04-96-1-0443 (G.D.S.), and the David and Lucile Packard Foundation (J.Y.Y.). W.W.L. thanks the National Science Foundation for a Postdoctoral Fellowship in Chemistry. J.S.L. acknowledges the support of a MIT/Merck Graduate Fellowship. We thank Professors J. Israelachvili (UCSB) and D. J. Pine (UCSB) for fruitful discussions and Mehul P. Shah (MIT) for technical assistance. We appreciate the donation of Pluronic P123 by BASF (Mt. Olive, NJ).

CM991097V